Natural Convection in a Tilted Isosceles Triangular Enclosure with Discrete Bottom Heating

Goutam Saha[1], Md. Tofiqul Islam[2], Sumon Saha[3] and Md. Quamrul Islam[4]
[1]Lecturer, Department of Related Subjects
Ahsanullah University of Science and Technology, Dhaka-1215, Bangladesh
[2,3]Lecturer, [4]Professor, Department of Mechanical Engineering
Bangladesh University of Engineering and Technology, Dhaka-1000, Bangladesh
Email: [1]rana_math06@yahoo.com, [2]mtislam@me.buet.ac.bd, [3]sumonsaha@me.buet.ac.bd,
[4]quamrul@me.buet.ac.bd

Abstract

A numerical study of natural convection in tilted isosceles triangular enclosure filled with air is presented by using a finite element based adapting meshing technique. In this present study, two upper walls are maintained at constant cold temperature, whereas a constant heat flux is symmetrically embedded at the bottom wall, and the non-heated parts of the bottom wall are considered adiabatic. The Grashof number based on the enclosure height is varied from 10^3 to 10^6. This study reports the effect of various aspect ratios, ranging from 0.5 to 1, and inclination angles of the enclosure from 0° to 60°, on the thermo-fluid characteristics. Results are presented in the form of streamline and isotherm plots as well as the variations of the Nusselt number and maximum temperature at the heat source surface under different conditions.

Keywords: Natural convection, triangular enclosure, aspect ratio, heat flux, finite element method.

1. Introduction

Natural convection heat transfer and fluid flow in enclosed spaces has been studied extensively in recent years in response to energy-related applications, such as thermal insulation of buildings using air gaps, solar energy collectors, furnaces and fire control in buildings and so on. The enclosures encountered in these applications are highly diverse in their geometrical configurations and most investigated enclosures include the annulus between horizontal cylinders, the spherical annulus, the closed rectangular cavity and the hollow horizontal cylinder. Effective cooling of electronic components has become increasingly important as power dissipation and component density continue to increase substantially with the fast growth of electronic technology. It is very important that such cooling systems are designed in the most efficient way and the power requirement for the cooling is minimized. The electronic components are treated as heat sources embedded on flat surface [1, 2]. In many applications natural convection is the only feasible mode of cooling of the heat source.

Several earlier studies have been performed for triangular enclosures in general [3 – 5], but the focus of this paper is on isosceles triangular enclosures with discrete heating from below. In modeling natural convection inside an isosceles triangular enclosure, nearly every numerical study previously reported in the literature employed a symmetry condition at the midplane and performed the simulations using only one half of the physical domain. Akinsete and Coleman [6] used a finite difference representation of the steady-state stream function, vorticity, and energy equations with an adiabatic boundary condition for the vertical wall in a right triangular enclosure, and made the claim that the problem could also represent the case for an isosceles triangular enclosure due

to symmetry. Poulikakos and Bejan [7] used a similar numerical approach, except that transient simulations were performed and an actual symmetry condition was used at the midplane for Gr up to 10^5 and A = 0.2 to 1.0. The use of the symmetry condition for this problem was continued by Ghassemi and Roux [8], Salmun [9], and Hasani and Chung [10]. Del Campo et al. [11] numerically modeled natural convection in triangular enclosures using a Galerkin finite element method with a stream function-vorticity formulation of the steady-state cases. They considered symmetric boundary conditions and heating from below, and no symmetry assumption was made. Triangular elements with linear interpolation were used, and the resulting graded mesh was symmetric. The solutions obtained were all symmetric about the midplane.

A continuing source of discrepancies in the literature is the calculation of average Nu (average dimensionless temperature gradient) along the base for the triangular enclosure. Akinsete and Coleman [6] recognized the existence of unbounded heat transfer at the corner of the enclosure where a temperature discontinuity exists, and calculated the limiting value of Nu using a method outlined by Collatz [12]. Poulikakos and Bejan [7] proposed starting the integration of the temperature gradient from a set distance away from the corner, thereby avoiding the singularity. Del Campo et al. [11] proposed a convective Nu defined as the difference between Nu for the case considered and Nu for pure conduction (using the same grid resolution). Salmun [9] and Hasani and Chung [10] did not specifically discuss the problem of the singularity and reported similar results for their average Nu due to having used the same grid resolutions. A limited number of laboratory experiments have been conducted for natural convection in triangular enclosures with base heating. One experiment reported in the literature, involving symmetric temperature boundary conditions for an isosceles triangular enclosure and base heating, was done by Flack [13]. The flow was reported as "turbulent" for $Gr = 3 \times 10^5$ with A = 0.58 and for $Gr = 8.9 \times 10^5$ with A = 1.0. Nu values were inferred using a Wollaston prism Schlieren interferometer. Flow patterns were determined qualitatively using a particle-based visualization technique and quantitative measurements were taken using a laser velocimeter. For the heated base experiments, no mention was made as to the symmetry of the flow. Poulikakos and Bejan [14] conducted experiments in a right triangular enclosure with an insulated vertical wall, and noted that the flow phenomenon should be similar to that found in a symmetric triangular space.

In the present study, the response of the two-dimensional, non-linear system to changes in all parameters is explored numerically using finite element discretization schemes. First the physical model and finite element formulation are described and the results are discussed in detail. Finally, some concluding remarks are stated. The main purpose of this paper is to provide steady-state numerical results considering the entire triangular region. The effects of aspect ratio, inclination angle, and Grashof number on the flow structure and heat transfer are investigated. Results are presented in the form of streamline and isotherm plots.

2. Mathematical Model

The physical model considered here is shown in Fig. 1, along with the important geometric parameters. It consists of an isosceles triangular enclosure whose upper walls are cooled to a constant cold temperature, θ_c. The bottom wall has a discrete heat source with constant heat flux, q'', and length L. The remaining parts of the bottom wall are adiabatic. The dimensionless governing equations of continuity (1), momentum (2)-(3), and energy (4) for steady state laminar flow of an incompressible Boussinesq fluid with negligible viscous dissipation are as follows:

$$\frac{\partial U}{\partial X}+\frac{\partial V}{\partial Y}=0 \tag{1}$$

$$U\frac{\partial U}{\partial X}+V\frac{\partial U}{\partial Y}=-\frac{\partial P}{\partial X}+\left(\frac{\partial^2 U}{\partial X^2}+\frac{\partial^2 U}{\partial Y^2}\right)+(\mathrm{Gr}\sin\Phi)\,\theta \tag{2}$$

$$U\frac{\partial V}{\partial X}+V\frac{\partial V}{\partial Y}=-\frac{\partial P}{\partial Y}+\left(\frac{\partial^2 V}{\partial X^2}+\frac{\partial^2 V}{\partial Y^2}\right)+(\mathrm{Gr}\cos\Phi)\,\theta \tag{3}$$

$$U\frac{\partial \theta}{\partial X}+V\frac{\partial \theta}{\partial Y}=\frac{1}{\mathrm{Pr}}\left(\frac{\partial^2 \theta}{\partial X^2}+\frac{\partial^2 \theta}{\partial Y^2}\right) \tag{4}$$

The dimensionless parameters used for non-dimensionalizing the governing equations are defined as follows:

$$X=\frac{x}{W},\ Y=\frac{y}{W},\ U=\frac{u\,W}{\eta},\ V=\frac{v\,W}{\eta},$$
$$P=\frac{pW^2}{\rho\eta^2},\ \theta=\frac{T-T_c}{\Delta T},\ \Delta T=\frac{q''W}{k},$$
$$Gr=\frac{g\beta\Delta T\,W^3}{\eta^2},\ Pr=\frac{\eta}{\alpha} \quad (5)$$

The boundary conditions for the present problem are specified as follows:

$U = V = 0$ for all walls
$\theta = 0$ for upper walls

$$\frac{\partial\theta}{\partial Y}=\begin{cases}0, & \text{for } 0<X<0.5-\frac{\varepsilon}{2}\\ -1, & \text{for } 0.5-\frac{\varepsilon}{2}\le X\le 0.5+\frac{\varepsilon}{2}\\ 0, & \text{for } 0.5+\frac{\varepsilon}{2}<X<1\end{cases} \quad (6)$$

for the bottom wall only.

Also the dimensionless heat transfer parameter is symbolized as follows:

$$Nu_X=\frac{1}{\theta_S(X)}$$
$$Nu=\frac{1}{\varepsilon}\int_0^{\varepsilon}\frac{1}{\theta_S(X)}dX \quad (7)$$

where $\theta_s(X)$ is the local dimensionless temperature.

2.1 Finite Element Formulation

The velocity component and the temperature distributions and linear interpolation for the pressure distribution according to their highest derivative orders in the differential Eqs. (1)-(4) are:

$$U(X,Y)=N_\alpha U_\alpha \quad (8)$$
$$V(X,Y)=N_\alpha V_\alpha \quad (9)$$
$$\theta(X,Y)=N_\alpha T_\alpha \quad (10)$$
$$P(X,Y)=H_\lambda P_\lambda \quad (11)$$

where α = 1, 2, … …, 6; λ= 1, 2, 3; N_α as the element interpolation functions for the velocity components and the temperature, and H_λ the element interpolation function for the pressure. To derive the finite element equations, the method of weighted residual is applied to the Eqs. (1)-(4). We get:

$$\int_A N_\alpha\left(\frac{\partial U}{\partial X}+\frac{\partial V}{\partial Y}\right)dA=0 \quad (12)$$

$$\int_A N_\alpha\left(U\frac{\partial U}{\partial X}+V\frac{\partial U}{\partial Y}\right)dA=-\int_A H_\lambda\left(\frac{\partial P}{\partial X}\right)dA+\int_A N_\alpha\left(\frac{\partial^2 U}{\partial X^2}+\frac{\partial^2 U}{\partial Y^2}\right)dA+\int_A N_\alpha(Gr\sin\Phi)\theta\,dA \quad (13)$$

$$\int_A N_\alpha\left(U\frac{\partial V}{\partial X}+V\frac{\partial V}{\partial Y}\right)dA=-\int_A H_\lambda\left(\frac{\partial P}{\partial Y}\right)dA+\int_A N_\alpha\left(\frac{\partial^2 V}{\partial X^2}+\frac{\partial^2 V}{\partial Y^2}\right)dA+\int_A N_\alpha(Gr\cos\Phi)\theta\,dA \quad (14)$$

$$\int_A N_\alpha\left(U\frac{\partial\theta}{\partial X}+V\frac{\partial\theta}{\partial Y}\right)dA=\frac{1}{Pr}\int_A N_\alpha\left(\frac{\partial^2\theta}{\partial X^2}+\frac{\partial^2\theta}{\partial Y^2}\right)dA \quad (15)$$

where A is the element area. Gauss's theorem is then applied to Eqs. (13)-(15) to generate the boundary integral terms associated with the surface tractions and heat flux. Then Eqs. (13)-(15) become:

$$\int_A N_\alpha\left(U\frac{\partial U}{\partial X}+V\frac{\partial U}{\partial Y}\right)dA+\int_A H_\lambda\left(\frac{\partial P}{\partial X}\right)dA+\int_A\left(\frac{\partial N_\alpha}{\partial X}\frac{\partial U}{\partial X}+\frac{\partial N_\alpha}{\partial Y}\frac{\partial U}{\partial Y}\right)dA-\int_A(Gr\sin\Phi)N_\alpha\theta\,dA=\int_{S_0}N_\alpha S_x\,dS_0$$

$$\int_A N_\alpha\left(U\frac{\partial V}{\partial X}+V\frac{\partial V}{\partial Y}\right)dA+\int_A H_\lambda\left(\frac{\partial P}{\partial Y}\right)dA+\int_A\left(\frac{\partial N_\alpha}{\partial X}\frac{\partial V}{\partial X}+\frac{\partial N_\alpha}{\partial Y}\frac{\partial V}{\partial Y}\right)dA-\int_A(Gr\cos\Phi)N_\alpha\theta\,dA=\int_{S_0}N_\alpha S_y\,dS_0$$

$$\int_A N_\alpha\left(U\frac{\partial\theta}{\partial X}+V\frac{\partial\theta}{\partial Y}\right)dA+\frac{1}{Pr}\int_A\left(\frac{\partial N_\alpha}{\partial X}\frac{\partial\theta}{\partial X}+\frac{\partial N_\alpha}{\partial Y}\frac{\partial\theta}{\partial Y}\right)dA=\int_{S_w}N_\alpha\,q_w\,dS_w$$

Here Eqs. (13)-(14) specify surface tractions (S_x, S_y) along outflow boundary S_0 and Eq. (15) specifies velocity components and fluid temperature or heat flux that flows into or out from domain along wall boundary S_w. Substituting the element velocity component distributions, the temperature distribution, and the pressure distribution from Eqs. (8)-(11), the finite element equations can be written in the form:

$$K_{\alpha\beta,x}U_\beta + K_{\alpha\beta,y}V_\beta = 0 \tag{16}$$

$$K_{\alpha\beta\gamma,x}U_\beta U_\gamma + K_{\alpha\beta\gamma,y}V_\beta U_\gamma + M_{\alpha\mu,x}P_\mu + \left(S_{\alpha\beta,xx} + S_{\alpha\beta,yy}\right)U_\beta - (\mathrm{Gr}\sin\Phi)K_{\alpha\beta}\theta_\beta = Q_{\alpha,u} \tag{17}$$

$$K_{\alpha\beta\gamma,x}U_\beta V_\gamma + K_{\alpha\beta\gamma,y}V_\beta V_\gamma + M_{\alpha\mu,y}P_\mu + \left(S_{\alpha\beta,xx} + S_{\alpha\beta,yy}\right)V_\beta - (\mathrm{Gr}\cos\Phi)K_{\alpha\beta}\theta_\beta = Q_{\alpha,v} \tag{18}$$

$$K_{\alpha\beta\gamma,x}U_\beta\theta_\gamma + K_{\alpha\beta\gamma,y}V_\beta\theta_\gamma + \frac{1}{\mathrm{Pr}}\left(S_{\alpha\beta,xx} + S_{\alpha\beta,yy}\right)\theta_\beta = Q_{\alpha,T} \tag{19}$$

where the coefficients in element matrices are in the form of the integrals over the element area and along the element edges S_0 and S_w as:

$$K_{\alpha\beta,x} = \int_A N_\alpha N_{\beta,x}\,dA,$$

$$K_{\alpha\beta\gamma,y} = \int_A N_\alpha N_\beta N_{\gamma,y}\,dA,$$

$$K_{\alpha\beta,y} = \int_A N_\alpha N_{\beta,y}\,dA,$$

$$K_{\alpha\beta\gamma,x} = \int_A N_\alpha N_\beta N_{\gamma,x}\,dA,$$

$$K_{\alpha\beta} = \int_A N_\alpha N_\beta\,dA,$$

$$S_{\alpha\beta,xx} = \int_A N_{\alpha,x} N_{\beta,x}\,dA,$$

$$S_{\alpha\beta,yy} = \int_A N_{\alpha,y} N_{\beta,y}\,dA,$$

$$M_{\alpha\mu,x} = \int_A H_\alpha H_{\mu,x}\,dA,$$

$$M_{\alpha\mu,y} = \int_A H_\alpha H_{\mu,y}\,dA,$$

$$Q_{\alpha,u} = \int_{S_0} N_\alpha S_x\,dS_0,$$

$$Q_{\alpha,v} = \int_{S_0} N_\alpha S_y\,dS_0,$$

$$Q_{\alpha,T} = \int_{S_w} N_\alpha q_w\,dS_w.$$

These element matrices are evaluated in closed-form ready for numerical simulation. Details of the derivation for these element matrices are omitted herein for brevity. The derived finite element equations, Eqs. (16)-(19), are nonlinear. These nonlinear algebraic equations are solved by applying the Newton-Raphson iteration technique by first writing the unbalanced values from the set of the finite element Eqs. (16)-(19) as:

$$F_{\alpha,p} = K_{\alpha\beta,x}U_\beta + K_{\alpha\beta,y}V_\beta$$

$$F_{\alpha,u} = K_{\alpha\beta\gamma,x}U_\beta U_\gamma + K_{\alpha\beta\gamma,y}V_\beta U_\gamma + M_{\alpha\mu,x}P_\mu + (S_{\alpha\beta,xx} + S_{\alpha\beta,yy})U_\beta - (\mathrm{Gr}\sin\Phi)K_{\alpha\beta}\theta_\beta - Q_{\alpha,u}$$

$$F_{\alpha,v} = K_{\alpha\beta\gamma,x}U_\beta V_\gamma + K_{\alpha\beta\gamma,y}V_\beta V_\gamma + M_{\alpha\mu,y}P_\mu + (S_{\alpha\beta,xx} + S_{\alpha\beta,yy})V_\beta - (\mathrm{Gr}\cos\Phi)K_{\alpha\beta}\theta_\beta - Q_{\alpha,v}$$

$$F_{\alpha,T} = K_{\alpha\beta\gamma,x}U_\beta\theta_\gamma + K_{\alpha\beta\gamma,y}V_\beta\theta_\gamma + \frac{1}{\mathrm{Pr}}\left(S_{\alpha\beta,xx} + S_{\alpha\beta,yy}\right)\theta_\beta - Q_{\alpha,T}$$

This leads to a set of algebraic equations with the incremental unknowns of the element nodal velocity components, temperatures, and pressures in the form:

$$\begin{bmatrix} K_{uu} & K_{uv} & K_{uT} & K_{up} \\ K_{vu} & K_{vv} & K_{vT} & K_{vp} \\ K_{Tu} & K_{Tv} & K_{TT} & 0 \\ K_{pu} & K_{pv} & 0 & 0 \end{bmatrix} \begin{Bmatrix} \Delta u \\ \Delta v \\ \Delta T \\ \Delta p \end{Bmatrix} = - \begin{Bmatrix} F_{\alpha,u} \\ F_{\alpha,v} \\ F_{\alpha,T} \\ F_{\beta,p} \end{Bmatrix}$$

where

$$K_{uu} = K_{\alpha\beta\gamma,x}U_\gamma + K_{\alpha\gamma\beta,x}U_\gamma + K_{\alpha\beta\gamma,y}V_\beta + \left(S_{\alpha\beta,xx} + S_{\alpha\beta,yy}\right), K_{uv} = K_{\alpha\beta\gamma,y}U_\gamma, ,$$

$$K_{u\theta} = -\sin\Phi\, K_{\alpha\beta}, K_{up} = M_{\alpha\mu,x}, K_{vu} = K_{\alpha\beta\gamma,x}V_\gamma,$$

$$K_{vv} = K_{\alpha\beta\gamma,x}U_\beta + K_{\alpha\gamma\beta,y}V_\gamma + K_{\alpha\beta\gamma,y}V_\gamma + \left(S_{\alpha\beta,xx} + S_{\alpha\beta,yy}\right), K_{v\theta} = -\cos\Phi\ K_{\alpha\beta},$$

$$K_{vv} = K_{\alpha\beta\gamma,x}U_\beta + K_{\alpha\gamma\beta,y}V_\gamma + K_{\alpha\beta\gamma,y}V_\gamma + \left(S_{\alpha\beta,xx} + S_{\alpha\beta,yy}\right), K_{vp} = M_{\alpha\mu,y}, K_{\theta u} = K_{\alpha\beta\gamma,x}\theta_\gamma,$$

$$K_{\theta v} = K_{\alpha\beta\gamma,y}\theta_\gamma, K_{\theta\theta} = K_{\alpha\beta\gamma,x}U_\beta + K_{\alpha\beta\gamma,y}V_\beta + \frac{1}{Pr}\left(S_{\alpha\beta,xx} + S_{\alpha\beta,yy}\right), K_{\theta p} = 0, ,$$

$$K_{pu} = K_{\alpha\beta,x},\ K_{pv} = K_{\alpha\beta,y},\ K_{p\theta} = 0,\ K_{pp} = 0.$$

The iteration process is terminated if the percentage of the overall change compared to the previous iteration is less than the specified value.

3. Results and Discussion

Equations (1)-(4) with boundary conditions given above have been solved numerically using a finite element based adapting meshing technique. It provides smooth solutions at the interior domain including the corner regions. Six noded triangular elements are used in this paper since the six noded elements smoothly capture the non-linear variations of the field variables. All six nodes are associated with velocities as well as temperature. Only the corner nodes are associated with pressure. This means that a lower order polynomial is chosen for pressure which is satisfied through the continuity equation. Solutions are assumed to converge when the following convergence criteria is satisfied for every dependent variables at every point in the solution domain:

$$\left|\frac{\phi_{new} - \phi_{old}}{\phi_{old}}\right| \le 10^{-6}$$

Where ϕ represents a dependent variable U, V, P, and θ. The working fluid is chosen as air with Prandtl number, $Pr = 0.71$. The normalized length of the constant flux heat source at the bottom wall, ε = L/W, was varied from 0.2 to 0.8. For each value of ε, the Grashof number, Gr was varied from 10^3 to 10^6, the aspect ratio, A was varied from 0.5 to 1 and the inclination angle, Φ, was varied from 0° to 60°.

In order to obtain a grid independent solution, a grid refinement test is performed for $A = 1.0$, $Gr = 10^3$ with $\varepsilon = 0.2$ and $\Phi = 0°$. Fig. 2 shows the convergence of the average Nusselt number, Nu, at the heated surface with the grid refinement. It is observed that grid independence is achieved with 4082 elements where there is insignificant change in Nu.

In order to validate the numerical code, the results were compared with those reported by Holtzman et al. [15]. Figure 3 shows the comparison of streamline and isotherm of present model with that obtained by Holtzman et al. [15]. The agreement is found to be excellent which validates the present computations indirectly.

3.1 Flow and Thermal Fields Characteristics

The effects of aspect ratio and inclination angle on the flow and thermal fields in a triangular enclosure for the lower values of discrete heat source size and Grashof number are presented in Fig. 4. A Smaller aspect ratio of the triangular enclosure with minute heated strip gives the formation of two circulating cells of different intensity and opposite directions of rotation at $\Phi = 30°$. Due to the weaker intensity of the vortices, diffusion is the principal heat transfer mechanism. Increasing the aspect ratio makes the primary circulating cell spread inside the enclosure space, resulting in higher recirculation strength, and a pocket of fluid is trapped at the top vertex. Thus, diffusion heat

transfer becomes profound. At Φ = 60°, the expansion of the primary vortex inside the cavity suppresses the secondary vortex at the right alcove of the enclosure. This flow scenario indicates that the convective current is responsible for the heat transport mechanism. An increase in aspect ratio strengthens the primary vortex, but still there are pockets of fluid entrapped at the top and right corners of the triangular enclosure. Here, the heat transfer rate increases, though a major portion of the heat is carried out by diffusion rather than a convection heat transfer mechanism. At Φ = 30°, the isotherms indicates a diffusion heat transfer mechanism. As the aspect ratio increases, the temperature gradient becomes precipitous, indicating strong diffusion heat transfer. While tilted angle is 60°, at low value of aspect ratio, isotherms become nonlinear and a plume formation is visualized pointing towards the settlement of buoyancy driven natural convection currents. Further increases in aspect ratio imply that the heat transfer increases albeit convection is overwhelmed by the diffusion heat transfer mechanism.

Figure 5 also shows the influence of the aspect ratio and the inclination angle on the thermo-fluid characteristics inside the enclosure of larger discrete heat source size for higher values of Grashof number. In case of Φ = 30° and small aspect ratio, two circulating cells of relatively lower strength are formed. For higher values of Grashof number and inclination angle, the secondary vortex experiences oppression, due to the rapid growth of the primary vortex. Then the secondary vortex subsides and is entrapped at the right recess of the enclosure. Thereby convection heat transfer surmounts diffusion heat transfer. The isotherms also show the supremacy of buoyancy effect through prolonged plume formation.

The change of flow and heat transfer attributes inside a triangular enclosure of aspect ratio 0.5 and heat source size 0.4 for different values of Grashof number, while the inclination angle is fixed to 0°, is shown in Fig. 6(a). In the presence of the lower magnitude of Grashof number, two circulating cells of almost equal strength and reverse directions of motion are developed. With increasing of the buoyancy effect, the intensity of the circulating cells increases, which is a sign of the supremacy of convection heat transfer. The isotherms are similar for the Grashof number ranging from 10^3 to 10^5. At $Gr = 10^6$, a strong plume is formed, resulting in better thermal convection heat transfer.

Figure 6(b) shows the effect of the inclination angle on the natural convection heat transfer within the cavity. At Φ = 15°, a primary vortex of relatively higher strength and large size and a secondary vortex of weaker strength and small size, appear inside the enclosure. This type of flow situation indicates that convection is the key mode of heat transfer mechanism. As the enclosure, is tilted at higher inclination angles, the large circulating cell spreads over the space inside the triangular enclosure strengthening its circulation. And the secondary vortex located near the right corner of the enclosure becomes minute. Thereby, buoyancy dominated natural convection prevails here. The isotherms show similar temperature distribution profiles within the enclosure for all values of the inclination angle. The evolution of the plume formation signifies that convective current is dominant.

3.2 Heat Transfer Analysis

The variation of average Nusselt number and maximum non-dimensional temperature along with Grashof number for different values of discrete heated strip is reported in Fig. 7 and 8. In general, the average Nusselt number remains invariant up to a certain value of Grashof number and then increases briskly with increasing Grashof number. Maximum Nu is obtained at small heat source size for higher value of Gr while Φ = 60°. Maximum non-dimensional temperature of the heat source does not change up to a certain value of Gr. After that it changes its profile as Gr increases. It is noticed that a lower value of θ_{max} is obtained at a higher value of Gr for all inclination angles. Therefore, better thermal performance is achieved for the triangular enclosure of small heat source size at higher Grashof number and inclination angle.

4. Conclusions

Two dimensional, steady, natural convection flow in a tilted isosceles triangular enclosure, partially subjected to constant heat flux at the bottom wall while the upper walls are cooled at a constant temperature, has been investigated numerically for a wide range of

Grashof numbers, aspect ratio of the enclosure, discrete heat source size and inclination angles. The synopsis of the investigation is that average Nusselt number decreases as the heated strip enlarges, and increases along with inclination angle. Optimum heat transport phenomenon is gained for higher value of Grashof number and aspect ratio of the enclosure.

NOMENCLATURE

A	aspect ratio *(H/W)*
g	gravitational acceleration [m/s^2]
Gr	Grashof number
H	height of the cavity [m]
k	thermal conductivity [W/m^{2}K]
L	length of the heat source [m]
Nu	Nusselt number
p	pressure [Pa]
P	dimensionless pressure
Pr	Prandtl number
q''	Heat flux at the source
T	Temperature [K]
ΔT	Temperature difference [K]
u,v	dimensional velocity [m/s]
U,V	dimensionless velocity
W	length of the cavity [m]
x,y	dimensional coordinates
X,Y	non-dimensional coordinates

Greek Symbols:

α	Thermal diffusivity [m^2/s]
β	Thermal expansion coefficient [1/K]
ε	discrete heat source size *(L/W)*
θ	Dimensionless temperature
ρ	Fluid density [kg/m^3]
η	Kinematic viscosity [m^2/s]
Φ	Inclination angle [deg]

Subscripts:

c	cold wall
s	local
max	max

5. References

[1] Incropera, F.P., Convection Heat Transfer in Electronic Equipment Cooling, ASME J. Heat Transfer Vol.110, pp. 1097-1111, 1988.

[2] Jaluria, Y., Natural Convection Cooling of Electronic Equipment. in Natural Convection: Fundamental and Applications (Edited by S. Kakac et al.), pp. 961-986. Hemisphere, Washington, D. C., 1985.

[3] Flack, R.D., Konopnicki, T.T., and Rooke, J.H., The Measurement of Natural Convective Heat Transfer in Triangular Enclosures, ASME J. Heat Transfer, Vol.101, pp. 648–654, 1979.

[4] Karyakin, Y.E., and Sokovishin, Y.A., Unsteady Natural Convection in a Triangular Enclosure, Fluid Dyn., Vol.20, pp. 811–815, 1985.

[5] Karyakin, Y.E., Sokovishin, Y.A., and Martynenko, O.G., Transient Natural Convection in Triangular Enclosures, Int. J. Heat Mass Transfer., Vol.31, pp. 1759–1766, 1988.

[6] Akinsete, V.A., and Coleman, T.A., Heat Transfer by Steady Laminar Free Convection in Triangular Enclosures, Int. J. Heat Mass Transfer., Vol.25, pp. 991–998, 1982.

[7] Poulikakos, D., and Bejan, A., The Fluid Dynamics of an Attic Space, J. Fluid Mech., Vol.131, pp. 251–269, 1983.

[8] Ghassemi, M., and Roux, J.A., Numerical Investigation of Natural Convection within a Triangular Shaped Enclosure, Heat Transfer in Convective Flows, R. K. Shah, ed., ASME, New York, pp. 169–175, 1989.

[9] Salmun, H., Convection Patterns in a Triangular Domain, Int. J. Heat Mass Transfer., Vol.38, pp. 351–362, 1995.

[10] Hasani, S.M.F., and Chung, B.T.F., Laminar Natural Convection in a Triangular Enclosure, Proceedings of the ASME Ocean Engineering Division, D.T. Valentine, and C.C. Jahnke, eds., ASME, New York, pp. 107–116, 1997.

[11] Del Campo, E.M., Sen, M., and Ramos, E., Analysis of Laminar Natural Convection in a Triangular Enclosure, Numer. Heat Transfer, Vol.13, pp. 353–372, 1988.

[12] Collatz, L., The Numerical Treatment of Differential Equations, Springer-Verlag New York, 1966.

[13] Flack, R.D., The Experimental Measurement of Natural Convection Heat Transfer in Triangular Enclosures Heated or Cooled From Below, ASME J. Heat Transfer, Vol.102, pp. 770–772, 1980.

[14] Poulikakos, D., and Bejan, A., Natural Convection Experiments in a Triangular Enclosure, ASME J. Heat Transfer, Vol.105, pp. 652–655, 1983.

[15] Holtzman, G.A., Hill, R.W., and Ball, K.S., Laminar Natural Convection in Isosceles Triangular Enclosures Heated from Below and Symmetrically Cooled from Above, ASME J. Heat Transfer, Vol.122, pp. 485–491, 2000.

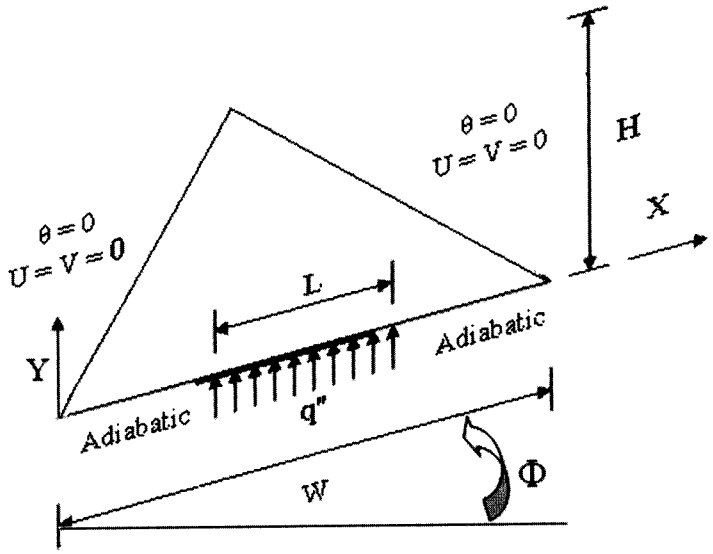

Fig. 1: Schematic diagram of the physical domain and boundary conditions

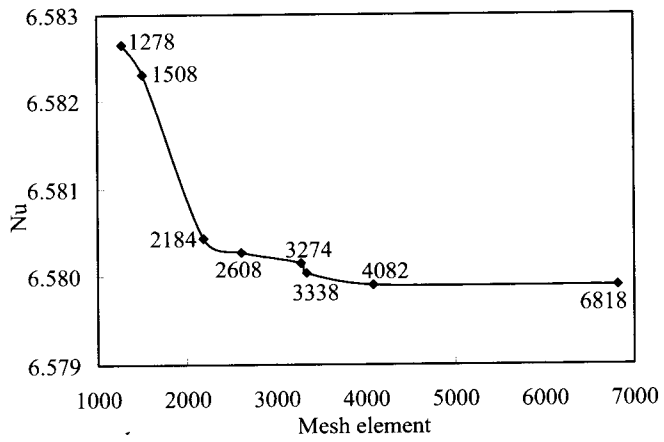

Fig. 2: Convergence of Nusselt number with mesh number for $A = 1$, $Gr = 10^3$ with $\varepsilon = 0.2$ and $\Phi = 0°$

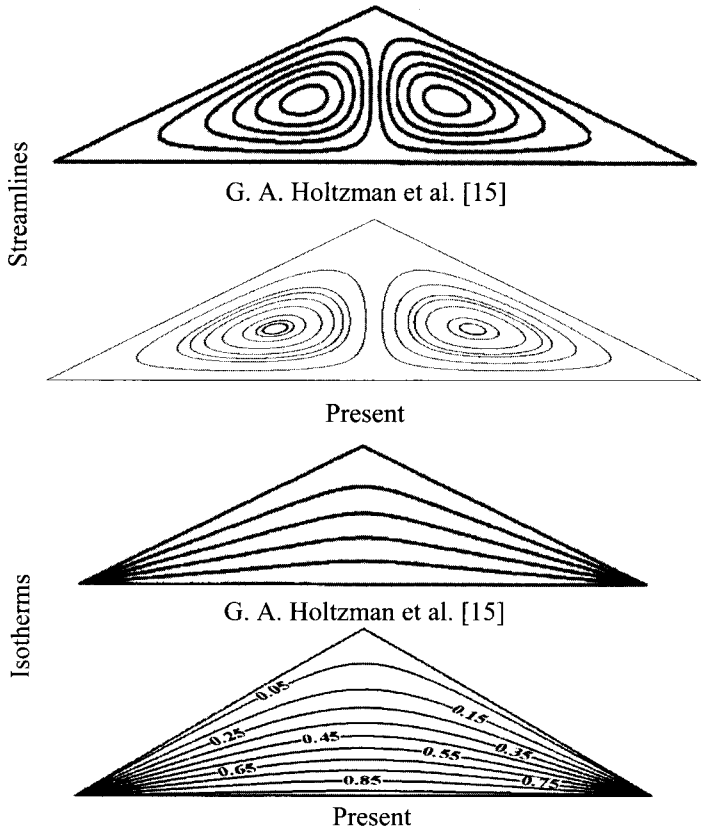

Fig. 3: Comparison of streamlines and isotherms for validation at $A = 0.5$, $\Phi = 0°$, $Gr = 10^3$ with the results of Holtzman et al. [15]

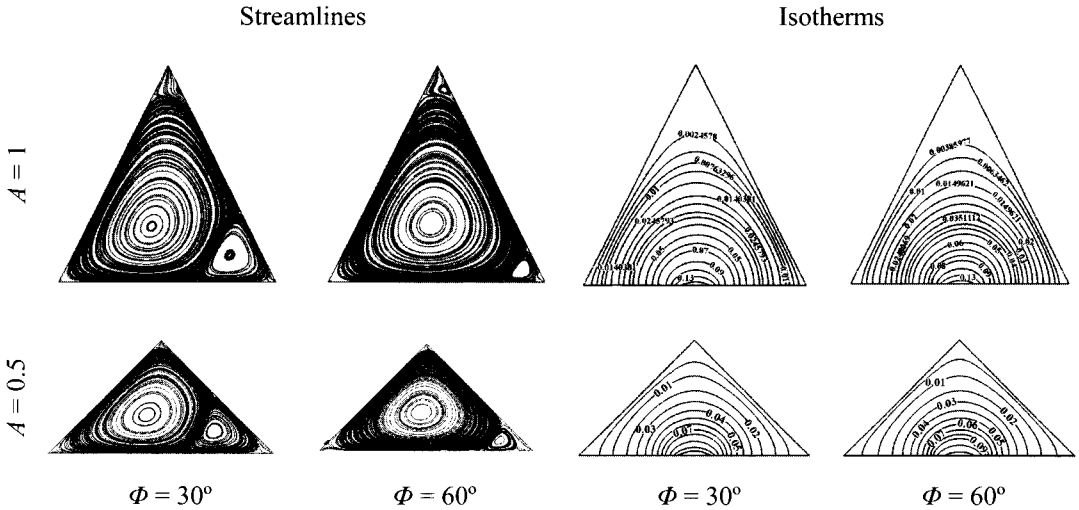

Fig. 4: Streamlines and isotherms in the enclosure with $\varepsilon = 0.2$ and $Gr = 10^4$

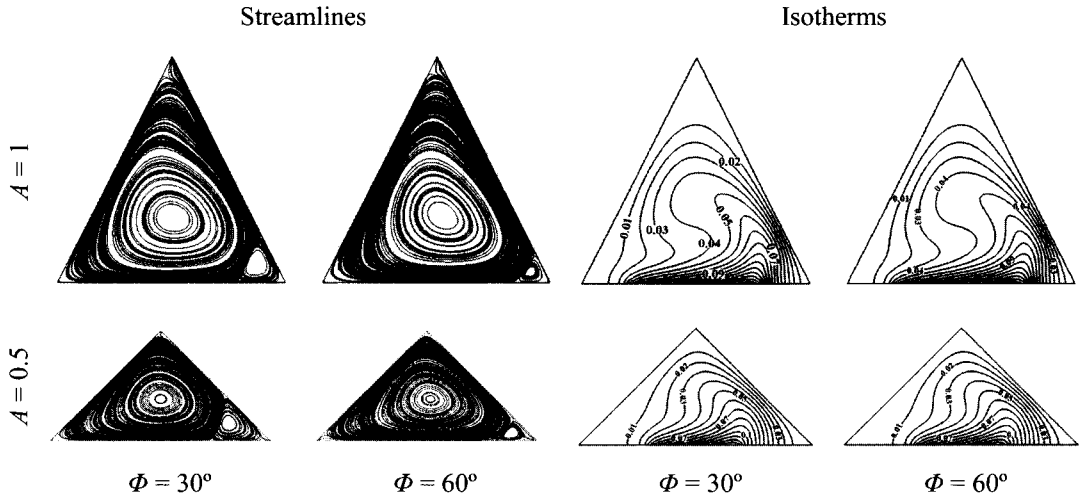

Fig. 5: Streamlines and isotherms in the enclosure with $\varepsilon = 0.6$ and $Gr = 10^6$.

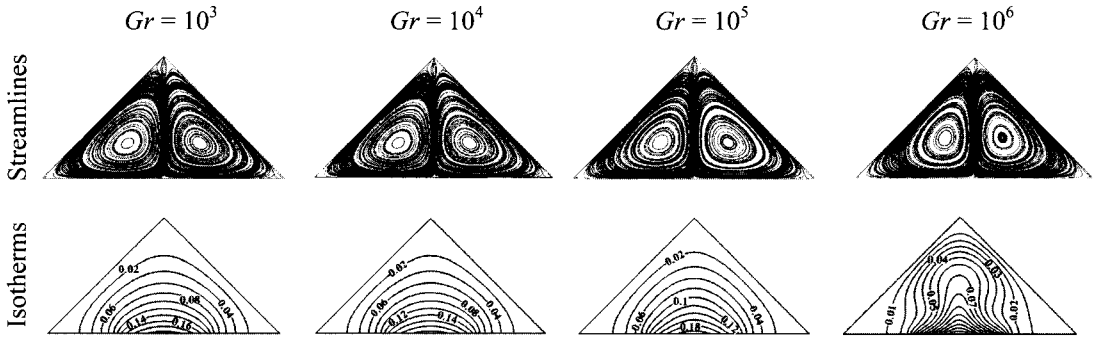

Fig.6 (a): Streamlines and isotherms in the enclosure with $\varepsilon = 0.4$, $\Phi = 0^O$ and $A = 0.5$

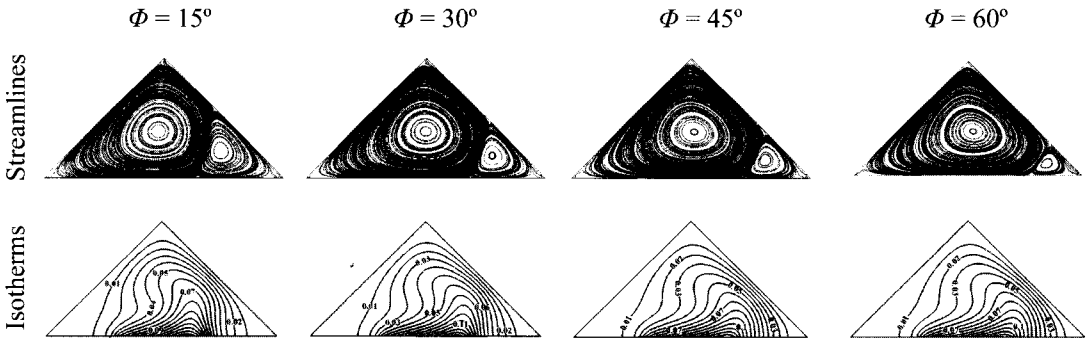

Fig. 6 (b): Evolution of the flow in the enclosure with inclination angles ($Gr = 10^6$, $A = 0.5$, $\varepsilon = 0.4$)

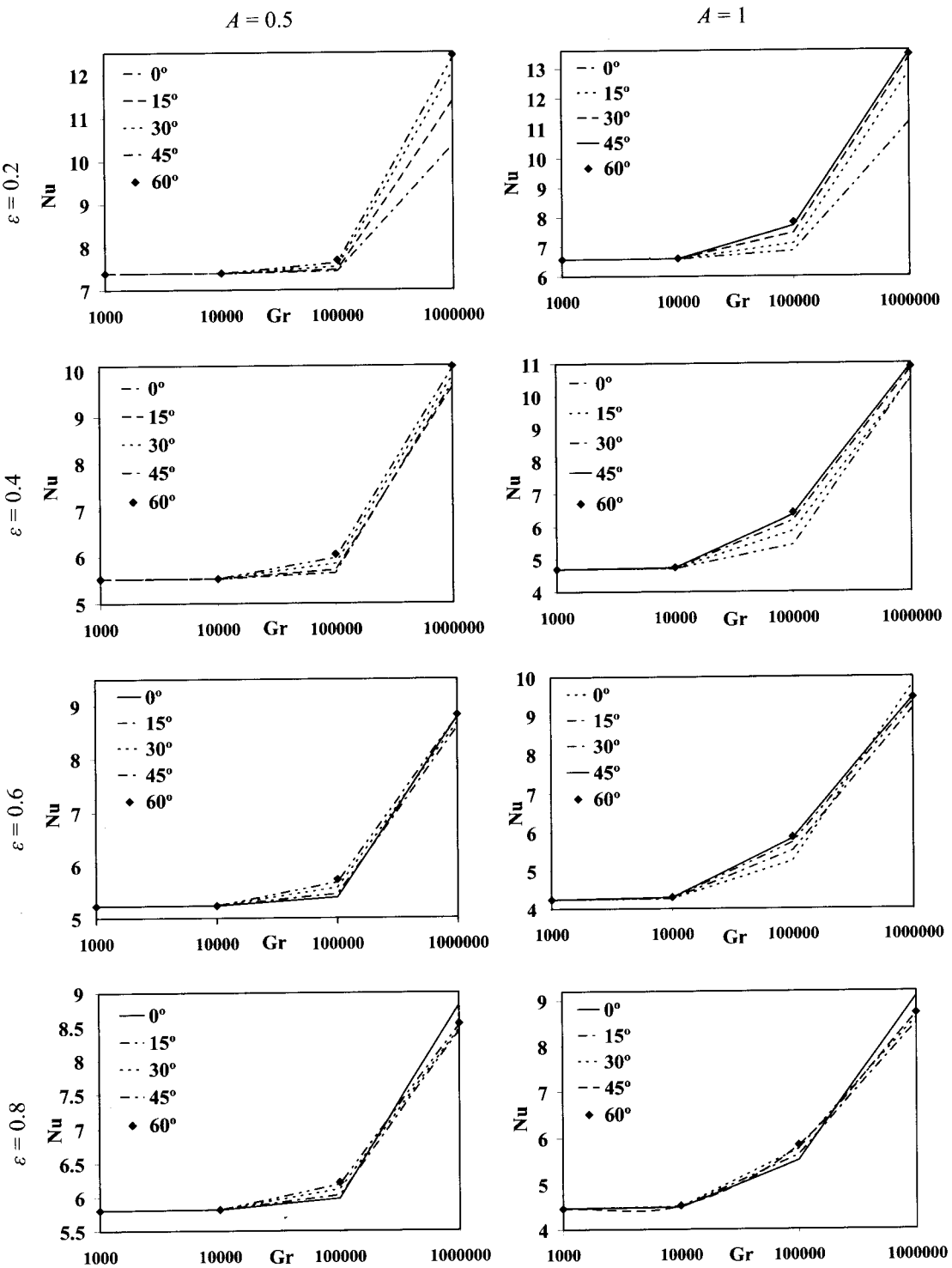

Fig. 7: Variation of the Nusselt number at the heated surface with Grashof number.

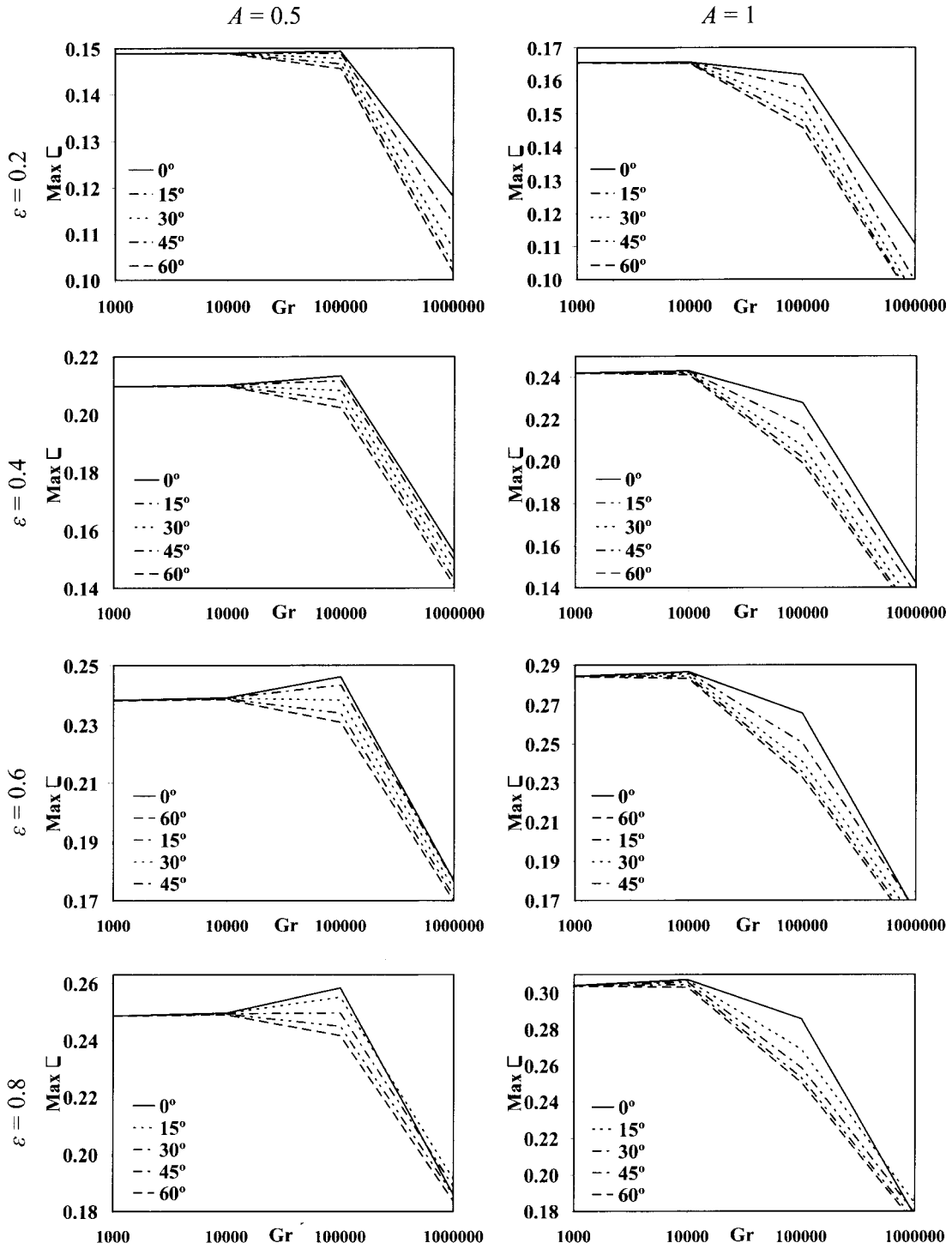

Fig. 8: Variation of the θ_{max} at the heated surface with Grashof number.